First principles local pseudopotential for silver: Towards orbital-free density-functional theory for transition metals

Baojing Zhou[a)]
Department of Chemistry and Biochemistry, University of California, Los Angeles, California 90095-1569

Emily A. Carter[b)]
Department of Chemistry and Biochemistry, University of California, Los Angeles, California 90095-1569 and Department of Mechanical and Aerospace Engineering and Program in Applied and Computational Mathematics, Princeton University, Princeton, New Jersey 08544

(Received 22 November 2004; accepted 3 March 2005; published online 12 May 2005)

Orbital-free density-functional theory (OF-DFT) with modern kinetic-energy density functionals (KEDFs) is a linear scaling technique that accurately describes nearly-free-electron-like (main group) metals. In an attempt towards extending OF-DFT to transition metals, here we consider whether OF-DFT can be used effectively to study Ag, a metal with a localized *d* shell. OF-DFT has two approximations: use of a KEDF and local pseudopotentials (LPSs). This paper reports construction of a reasonably accurate LPS for Ag by means of inversion of the Kohn–Sham (KS) DFT equations in a bulk crystal environment. The accuracy of this LPS is determined within KS-DFT (where the exact noninteracting kinetic energy is employed) by comparing its predictions of bulk properties to those obtained from a conventional (orbital-based) nonlocal pseudopotential (NLPS). We find that the static bulk properties of fcc and hcp Ag predicted within KS-DFT using this LPS compare fairly well to those predicted by an NLPS. With the transferability of the LPS established, we then use this LPS in OF-DFT, where several approximate KEDFs were tested. We find that a combination of the Thomas–Fermi (T_{TF}) and von Weizsäcker (T_{vW}) functionals ($T_{\mathrm{vW}}+0.4T_{\mathrm{TF}}$) produces better densities than those from the linear-response-based Wang–Teter KEDF. However, the equations of state obtained from both KEDFs in OF-DFT contain unacceptably large errors. The lack of accurate KEDFs remains the final barrier to extending OF-DFT to treat transition metals. © *2005 American Institute of Physics*. [DOI: 10.1063/1.1897379]

I. INTRODUCTION

Currently in condensed-matter physics, the most accurate mean-field electronic structure method is the density-functional theory (DFT).[1] When it was first proposed, a major obstacle for the original DFT was the need for density functionals that could accurately represent the kinetic energy. To surmount this problem, Kohn and Sham (KS) introduced a set of fictitious one-electron orbitals, namely, the so-called KS orbitals, so that the kinetic energy of an interacting system could be approximated by the exact kinetic energy of a set of noninteracting electrons with the same density.[2] The remaining deficit in the kinetic energy, namely, the difference between the full interacting system's kinetic energy and the KS noninteracting system's kinetic energy, is expected to be accounted for in the electron exchange-correlation functional. Subsequent advances in accurate representations of the exchange-correlation functional served to establish the reliability of Kohn–Sham density-functional theory (KS-DFT) for a wide class of molecules and materials.[3] A further advance came with the development of reliable nonlocal pseudopotentials (NLPSs)[4] to represent the electron-ion interaction, which reduced the cost of KS-DFT calculations by treating only the valence electrons explicitly. These NLPSs achieve quite high accuracy by means of orbital-based projection operators that allow different potentials to be felt by electrons of different angular momentum.

Orbital-based KS-DFT typically scales as $O(N_k \cdot N^3)$, where N is a measure of system size (basis set size and number of occupied orbitals) and N_k is the number of the **k** points used in the Brillouin-zone (BZ) sampling required for periodic systems.[5] Recently, both massively parallel (see, e.g., Ref. 6) and linear scaling (Ref. 7) algorithms for KS-DFT have allowed systems of more than 1000 atoms to be studied.[6,8] However, such orbital-based linear scaling algorithms only work for insulators, since they rely on the nearsightedness principle of Kohn[9] that leads to sparse density matrices. Metallic systems will not exhibit linear scaling with such algorithms, and BZ sampling in such metallic crystals is extremely expensive (N_k can easily be of the order of 1000). Therefore, alternative algorithms for solving the DFT equations for metals are needed. Such a scheme is provided by orbital-free density-functional theory (OF-DFT), which solves directly for the electron density instead of a set of orbitals. As a result, BZ sampling is eliminated (and hence

[a)]Current address: Department of Chemistry, University of British Columbia, 2036 Main Mall, Vancouver, BC V6T 1Z1, Canada.
[b)]Electronic mail: eac@princeton.edu

its order 1000 prefactor) and there is only one equation to solve, namely, the Thomas–Fermi–Hohenberg–Kohn (TFHK) equation[1]

$$\frac{\delta E_v[\rho]}{\delta \rho(\mathbf{r})} = \frac{\delta T_s[\rho]}{\delta \rho(\mathbf{r})} + \frac{\delta E_H[\rho]}{\delta \rho(\mathbf{r})} + \frac{\delta E_{xc}[\rho]}{\delta \rho(\mathbf{r})} + v(\mathbf{r}) = \mu. \quad (1)$$

Here T_s is the kinetic energy of a noninteracting system of electrons the density of which is the same as the interacting electron system, E_H is the classical Hartree repulsion energy, E_{xc} is the exchange-correlation energy (again, E_{xc} also includes the difference between the interacting and noninteracting kinetic energies), and v is the external potential (typically, the electron-nuclear attraction term), while μ is the Lagrange multiplier that guarantees the correct normalization of the electron density during the minimization and corresponds to the chemical potential after the total energy $E_v[\rho]$ is minimized. This equation can be solved in a linear or near-linear scaling fashion,[10] with no crossover between $N_k \cdot N^3 \rightarrow N$ or $N \ln N$ scaling, as in orbital-based linear scaling algorithms. Quite sometime ago, in fact, OF-DFT was used to examine the dynamics of several thousand atoms near a metallic grain boundary.[11] This illustrates the speed and efficiency of the method, as does its recent use in a multiscale model of nanoindentation.[12]

The drawbacks of OF-DFT lie in the two necessary approximations for the kinetic energy and the electron-ion interaction. To ever compete effectively with KS-DFT, OF-DFT research must focus on developing accurate kinetic-energy density functionals (KEDFs)[13–20] and reliable local pseudopotentials (LPSs),[14,21–24] since the orbital-dependent NLPSs cannot be employed in OF-DFT. In the last decade, high-quality KEDFs based on linear-response (LR) theory[5,25] have been derived for main group metallic systems.[16–20] OF-DFT calculations on nearly-free-electron-like metals, using these linear-response kinetic-energy density functionals (LR KEDFs) coupled with reliable LPSs,[21–24] are capable of reproducing KS-DFT results quite closely, with errors on the order of meV/atom.[20]

Encouraged by the success of OF-DFT for simple metals, our objective now is to further extend this method to covalent materials[15] and transition metals. As usual, the major obstacles are representations of the KEDF and the LPS. Recently, we developed a new method to generate first-principles bulk LPSs (BLPSs) that are one-to-one mapped to target bulk densities (exploiting the first Hohenberg–Kohn theorem[1]) by inverting the KS equations in a bulk crystal environment.[23] A highly transferable BLPS was produced for bulk Si using this method. Here we apply this same pseudopotential construction method to bulk Ag (where we will treat explicitly the valence d and s electrons), as a first step toward extending OF-DFT to describe bulk transition metals.

II. CONSTRUCTION OF A BLPS FOR Ag

All KS-DFT calculations performed here use the local-density approximation (LDA) for electron exchange and correlation. The LDA is based on quantum Monte Carlo results of Ceperley and Alder,[26] as parametrized by Perdew and Zunger.[27]

We construct the BLPS for Ag in KS-DFT by following the procedure laid out in Ref. 23, which we now outline briefly. First, the Wang–Parr (WP)[28] iterative scheme is used within bulk crystal KS-DFT calculations to obtain atomic form factors,[29] which define the BLPS at different Bragg vectors in reciprocal space (see Secs. II A–II C). This procedure will be reviewed briefly in Sec. II D (see Ref. 23 for details). We then construct the BLPS from the atomic form factors, ensuring a correct Coulombic tail for the LPS. The second step is more complex for Ag than it was for our earlier work on Si; further details are provided in Sec. II E.

A. Pseudopotentials

The target bulk densities required for the WP iterations are obtained from KS-DFT calculations using a Troullier–Martins (TM) norm-conserving NLPS[30] for Ag atom in its ground state $4d^{10}5s^1$ configuration, generated within the FHI98PP[31] code. Default values of the core cutoff radii r_c were used for the s,p, and d channels: 2.419, 2.603, and 2.419 bohr, respectively. As usual, this Troullier–Martins nonlocal pseudopotential (TM NLPS) is set up in the Kleinman–Bylander form,[32] containing a nonlocal part and a local part, with the latter chosen to be a mixture of 95% s and 5% d to avoid the so-called ghost state problem.[33]

A modified version of the FHI98PP code was used to generate a corresponding atomic LPS (ALPS),[34] analogously constructed by inversion of the KS equations for the atom, such that it can reproduce the target atomic KS density obtained using the TM NLPS. This ALPS is used as an initial guess for the WP iterative scheme. After the atomic form factors are obtained, many versions of the BLPS were constructed until an optimal BLPS yielded satisfactory bulk properties in KS-DFT calculations. Testing many versions of the BLPS is necessary because the inversion process is an under-determined problem, yielding no unique solution. Figure 1(a) plots in real space the short-range parts of the ALPS and our final (best) BLPS. Figure 1(b) depicts a wider range for the ALPS, the final optimal BLPS, as well as the TM NLPS. These pseudopotentials will be compared in more detail below.

B. Calculational details for construction and testing of the BLPS

First, the equilibrium structures of the ground-state face-centered-cubic (fcc) phase and a hypothetical hexagonal-close-packed (hcp) phase of bulk Ag are calculated using the TM NLPS within Kohn–Sham density-functional theory local-density approximation (KS-DFT-LDA) in the CASTEP[35] code. The target densities for the WP iterative scheme are then generated for these two structures. Primitive one-atom fcc and two-atom hcp cells are employed in all KS calculations used to construct and test the BLPS. For the hcp primitive cell, the angles between the lattice vectors are $\alpha=\beta=90°$, $\gamma=120°$, the c/a ratio is predicted to be 1.656 (experimental value=1.63; Ref. 36), and the fractional coordinates of the two atoms are $\left(\frac{2}{3},\frac{1}{3},\frac{3}{4}\right)$ and $\left(\frac{1}{3},\frac{2}{3},\frac{1}{4}\right)$. A 1200-eV kinetic energy cutoff is used to represent the deep NLPS [see Fig. 1(b)] so that the total energy could be converged to

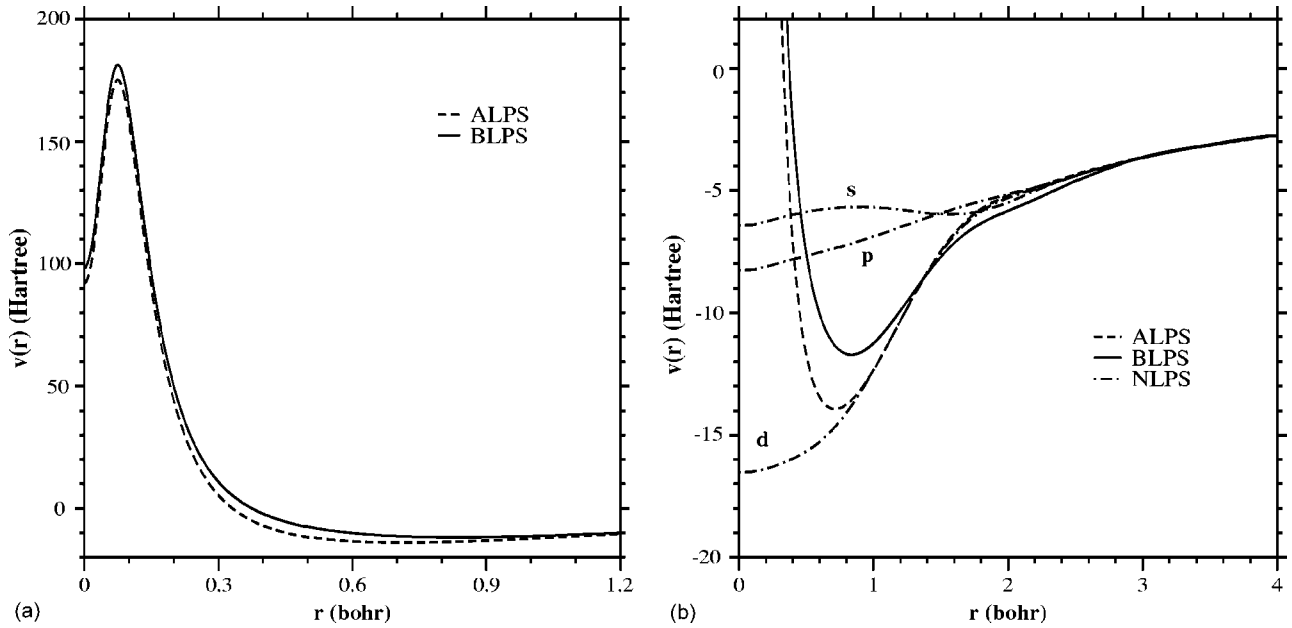

FIG. 1. (a) The real space ALPS (dashed) and BLPS (solid) at short range; (b) Comparison of the ALPS (dashed), BLPS (solid), and NLPS (dot-dashed), including s, p, and d-channels, over longer range. The NLPS, ALPS, and BLPS are Coulombic beyond 7.43, 7.43, and 8.5 bohr, respectively.

0.002 eV/atom, in order to resolve the very slight energy difference between fcc and hcp Ag. For such fine resolution, we require 84 and 96 irreducible **k** points for fcc and hcp primitive cells, respectively, generated using the Monkhorst–Pack method[37] for BZ sampling. Since they are metallic phases, Fermi-surface smearing is invoked to converge the KS orbitals at the Fermi level, with a smearing width of 0.1 eV.

A modified version of the CASTEP[35] code is used to obtain the atomic form factors of the fcc and hcp phases. Since we only require convergence of the electron density in the WP iterative scheme to obtain the effective potential that returns our target density, we are able to use less irreducible **k** points just for this part of the construction (56 for fcc and 84 for hcp) in order to reduce the cost.

After the WP iterative procedure yields the atomic form factors, we construct the BLPS from the form factors and then work to further refine the BLPS, as described in Sec. II E. We find that KS-DFT total energies using the BLPS are not completely converged at a 1200-eV cutoff because the BLPS is extremely repulsive near the core [see Fig. 1(a)]. However, this does not affect the quality of our final BLPS, as demonstrated in calculations using an even larger kinetic-energy cutoff (see Sec. III). We find that the KS-BLPS total energies at different cell volumes are lowered by the same amount ($\sim$0.15 eV/atom), so that the shape of the equations of state (EOSs) of bulk Ag are not affected. As usual, it is easier to converge energy differences than absolute energies.

C. Kohn–Sham nonlocal pseudopotential (KS-NLPS) benchmark properties for crystalline Ag

The EOSs of fcc and hcp Ag predicted by KS-DFT with the NLPS are shown in Fig. 2, where we see they are nearly degenerate. The inset shows that the equilibrium energy of the fcc phase is slightly lower (by $\sim$10 meV/atom) than that of the hcp phase, as it should be.

To obtain static structural properties, the EOS data are fitted to Murnaghan's equation of state[38]

$$E_{\mathrm{tot}}(V) = \frac{B_0 V}{B_0'}\left(\frac{(V_0/V)^{B_0'}}{B_0' - 1} + 1\right) + \text{constant}, \tag{2}$$

where B_0 and B_0' are the bulk modulus and its pressure derivative at the equilibrium volume V_0, respectively. Table I displays our KS-NLPS equilibrium volumes, bulk moduli,

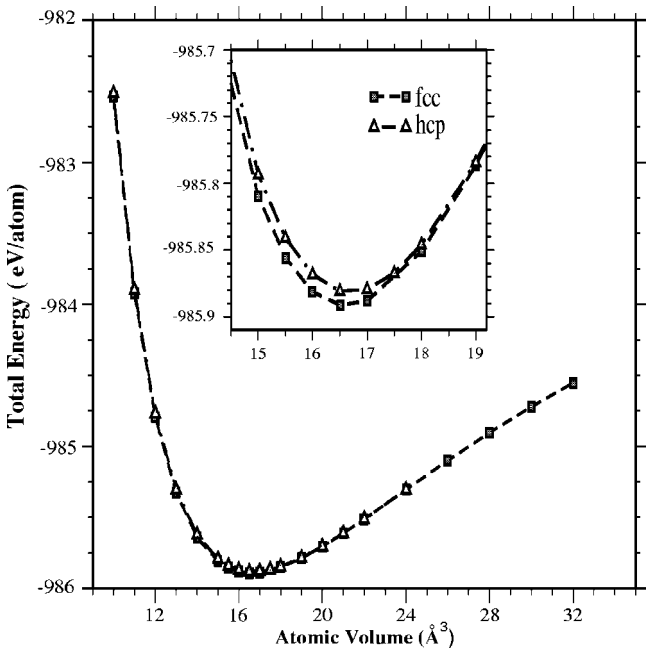

FIG. 2. KS-NLPS total energies (eV/atom) vs atomic volume (Å^3) for fcc (dark squares) and hcp (open triangles) Ag.

TABLE I. Comparison of various pseudopotential KS-LDA and experimental bulk properties for fcc and hcp Ag. Cohesive energies are not available using the BLPS (see Results of Sec. III for details); instead the equilibrium total energies per atom obtained from the Murnaghan fit are given in parentheses.

	V_0(Å^3)	B_0(GPa)	E_c(eV/atom)
NLPS			
fcc	16.848	116	3.445
hcp	16.880	121	3.442
BLPS			
fcc	17.084	130	NA(−1221.080)
hcp	17.610	143	NA(−1221.060)
Other work[a]			
fcc	17.417	96	3.01
hcp	17.495	103	3.01
Experimental[b]			
fcc	16.817	101	2.95

[a]From Ref. 39—KS-LDA/NLPS (HSC scheme).
[b]From Ref. 41. V_0 is extrapolated to 0 K, using the coefficient of thermal expansion for Ag (Ref. 42).

and cohesive energies (E_c, relative to the ground state $5s^1 4d^{10}$ Ag atom) for fcc and hcp Ag. Note that the Murnaghan fit yields an energy difference between the fcc and hcp phases that is slightly smaller than implied by the actual data in Fig. 2. Nevertheless, the Murnaghan fit still yields fcc as the ground-state structure for Ag. The properties predicted are consistent with other Kohn–Sham local-density approximation (KS-LDA)/NLPS calculations[39] (Table I), in which the NLPS was based on the Hamann–Schlüter–Chiang (HSC)[40] scheme and the basis set used included both plane waves and localized numerical functions. Our equilibrium volume is slightly better than that of Ref. 39, while their bulk modulus and cohesive energy are superior to ours, perhaps due to the more specialized basis set used. The experimental values[41] are shown for comparison. V_0 is obtained by extrapolating the room temperature V_0 from Ref. 41 to 0 K; B_0 is measured at room temperature, while E_c is for 0 K and 1 atm.

The KS-NLPS densities of fcc and hcp Ag at their equilibrium volumes will be used as the target densities that we will require the BLPS to match during iterative construction of the BLPS. Figure 3 displays contours of the density in the (100) plane of fcc Ag and (110) plane of hcp Ag. Most of the electron density is localized in the outer core (dark) region, as expected. These dark regions correspond to the ~10 $4d$ electrons, while the lighter regions reflect the density of the more delocalized $s(p)$ electrons.

D. Iterative BLPS construction procedure

In the WP iterative scheme,[28] the following KS equation:

$$\left(-\frac{1}{2}\nabla^2 + v_{\text{eff}}(\mathbf{r})\right)\phi_{i,k} = \epsilon_{i,k}\phi_{i,k}, \tag{3}$$

is inverted to obtain the local KS effective potential $v_{\text{eff}}(\mathbf{r})$, which is one-to-one mapped (according to the first Hohenberg–Kohn theorem[1]) to a given target density, $\rho(\mathbf{r})$. Here, i is the band index and k is the index of $\mathbf{k}$ points. During the WP iterations, the KS effective potential $v^n_{\text{eff}}(\mathbf{r})$ is updated at iteration step n via

$$v^n_{\text{eff}}(\mathbf{r}) = v^{n-1}_{\text{eff}}(\mathbf{r}) + \frac{\rho(\mathbf{r}) - \rho^n(\mathbf{r})}{\overline{\rho}^n(\mathbf{r})} = v^{n-1}_{\text{eff}}(\mathbf{r}) + \Delta v^n(\mathbf{r}). \tag{4}$$

Here $\rho^n(\mathbf{r})$ and $\overline{\rho}^n(\mathbf{r})$ are the nth iteration's density and energy-weighted density, with the latter defined as

$$\overline{\rho}^n(\mathbf{r}) = \sum_k w(k) \sum_i f^n_{i,k} \frac{|\phi^n_{i,k}(\mathbf{r})|^2}{\epsilon^n_{i,k}}, \tag{5}$$

where $w(k)$ is the weight associated with each $\mathbf{k}$ point and $f_{i,k}$ is the occupation number of the orbital $\phi_{i,k}$. As mentioned above, a similarly constructed ALPS is used as the initial guess $v^{n=1}_{\text{eff}}(\mathbf{r})$ for the WP scheme performed for the bulk

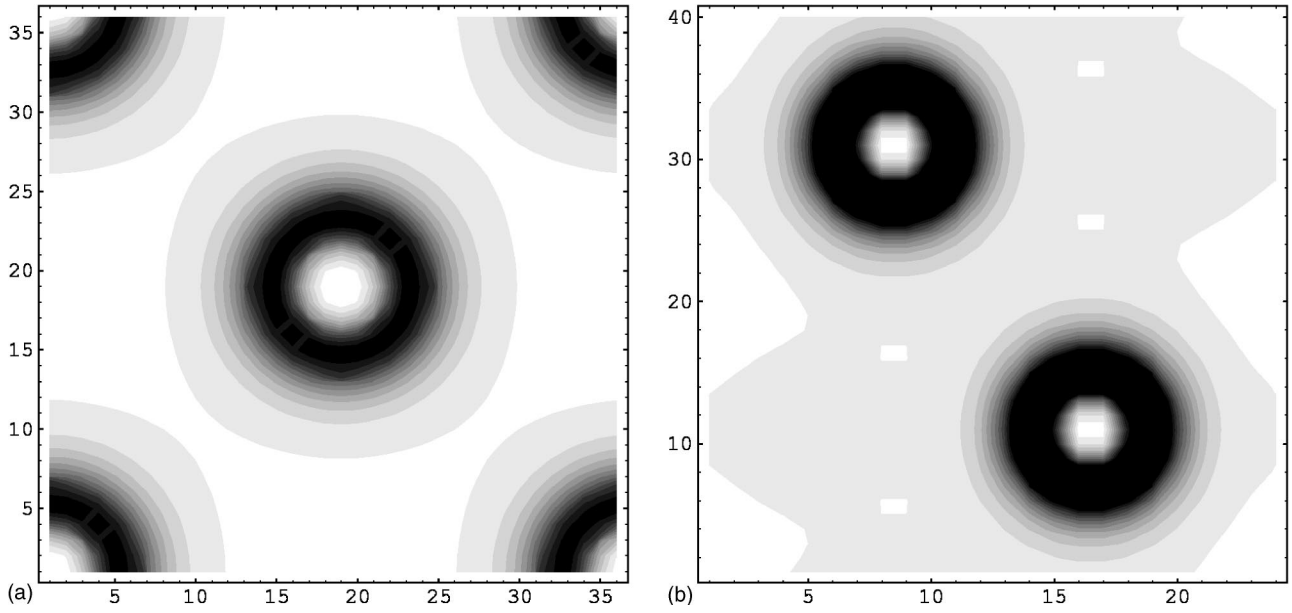

FIG. 3. Contour plot of KS-NLPS density. Dark areas represent high density, light areas low density. (a) (100) plane of fcc Ag; (b) (110) plane of hcp Ag.

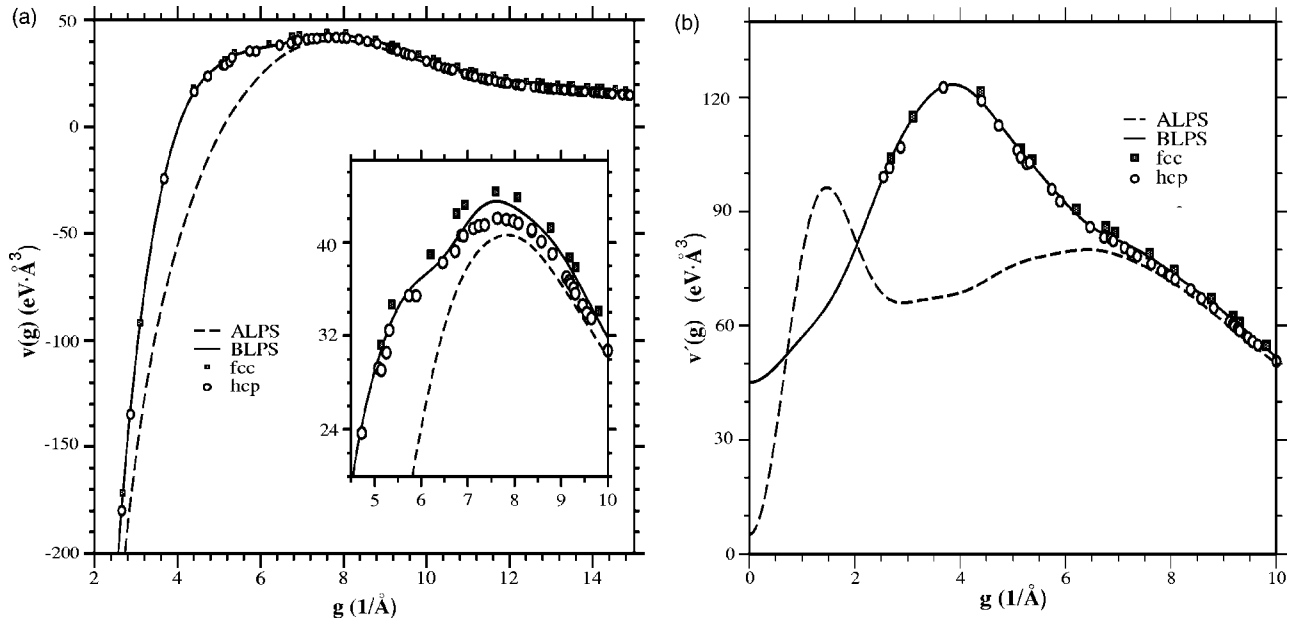

FIG. 4. The ALPS (dashed line), best BLPS (solid line), and form factors (symbols) of fcc (dark squares) and hcp (open circles) Ag obtained from the Wang–Parr method. (a) The full potential in reciprocal space [Eq. (9)]. Inset: enlargement of intermediate g-vector region. (b) The corresponding quantities without Coulombic contributions [Eq. (10)].

crystal. This initial KS effective potential is modified at each iterative step, based on Eq. (4), until the final effective potential reproduces the target density $\rho(\mathbf{r})$ within some threshold[23] (e.g., we require the Hartree energy $J[\Delta\rho]$ of the density difference $\Delta\rho(\mathbf{r})=\rho(\mathbf{r})-\rho^n(\mathbf{r})$ to be less than $\sim$0.1 meV/atom). Then we unscreen the final global KS effective potential $v_{\mathrm{eff}}^{\mathrm{global}}(\mathbf{r})$ by removing the Hartree and exchange-correlation potential due to the valence electrons, yielding a global LPS in real space

$$v_{\mathrm{loc}}^{\mathrm{global}}(\mathbf{r}) = v_{\mathrm{eff}}^{\mathrm{global}}(\mathbf{r}) - \frac{\delta J[\rho]}{\delta\rho} - \frac{\delta E_{\mathrm{xc}}[\rho]}{\delta\rho}, \tag{6}$$

where $J[\rho]$ and $E_{\mathrm{xc}}[\rho]$ are the usual Hartree Coulomb repulsion and exchange-correlation energies. By "global," we mean that this pseudopotential is spread out over every atom in the crystal.

Ultimately, we need an atom-centered pseudopotential so that it can be used in many different environments. We therefore transform $v_{\mathrm{PS}}^{\mathrm{global}}(\mathbf{r})$ to reciprocal space and divide by the structure factor $S(\mathbf{g})$,[5] yielding the pseudopotential form factor[29] $v^{\mathrm{atom}}(\mathbf{g})$ for fcc and hcp Ag, from which an atom-centered LPS will be derived,

$$v^{\mathrm{global}}(\mathbf{g}) = \frac{1}{\Omega}\int_{\Omega} v_{\mathrm{loc}}^{\mathrm{global}}(\mathbf{r})\cdot \mathrm{e}^{i\mathbf{g}\cdot\mathbf{r}}\mathrm{d}\mathbf{r}, \tag{7}$$

$$v^{\mathrm{atom}}(\mathbf{g}) = \frac{v^{\mathrm{global}}(\mathbf{g})}{S(\mathbf{g})}. \tag{8}$$

Note that in Eq. (7), Ω is usually the volume of the simulation cell, however, in CASTEP code, it is the number of grid points in the simulation cell so that $v^{\mathrm{global}}(\mathbf{g})$ is cell-size independent. Consequently, the units for $v^{\mathrm{global}}(\mathbf{g})$ are eV Å^3 instead of eV, as are the units of $v^{\mathrm{atom}}(\mathbf{g})$. We then spherically average the form factor $v^{\mathrm{atom}}(\mathbf{g})$ to get a one-dimensional (1D) isotropic pseudopotential form factor $v_{\mathrm{bulk}}(g)$

$$v_{\mathrm{bulk}}(g) = \frac{1}{n_g}\sum_{|\mathbf{g}_i|=g} v^{\mathrm{atom}}(\mathbf{g}_i), \tag{9}$$

where n_g is the total number of $\mathbf{g}$ vectors of equivalent length g.

This 1D form factor is depicted by the symbols in Fig. 4(a). At low g vectors, corresponding to large distances, the LPS is swamped by the Coulombic tail $\left(-\frac{4\pi Z}{g^2}\right)$ that the pseudopotential must ultimately obey. In order to increase the numerical sensitivity of our construction, we temporarily remove the Coulombic contribution to obtain $v'_{\mathrm{bulk}}(g)$

$$v'_{\mathrm{bulk}}(g) = v_{\mathrm{bulk}}(g) + \frac{4\pi Z}{g^2}, \tag{10}$$

shown by the symbols in Fig. 4(b). The inset of Fig. 4(a) reveals that especially in the region 6 Å$^{-1}<g<$10 Å^{-1}, the pseudopotential form factors of the two structures do not fall perfectly on a smooth curve, so that our choice for the BLPS must strike a compromise. For comparison, we also plot the ALPS, where we see large deviations between the ALPS and the pseudopotential form factors derived from the bulk crystal calculations. This hints at the improvement we expect upon moving from the ALPS to the BLPS (*vide infra*).

E. Constructing the BLPS from the form factors

We found that it is more difficult to construct a satisfactory BLPS for Ag than for Si. This is because the shapes of the EOSs for Ag are sensitive to the reciprocal space BLPS in two regions: $g<4.0$ Å^{-1} and 5.5 Å$^{-1}<g<$10.0 Å^{-1}, while those of Si are only sensitive to the reciprocal BLPS at the first few Bragg vectors. The strategy we take here is to vary the (unconstrained) shape of the reciprocal space BLPS in both regions and build many different versions of the

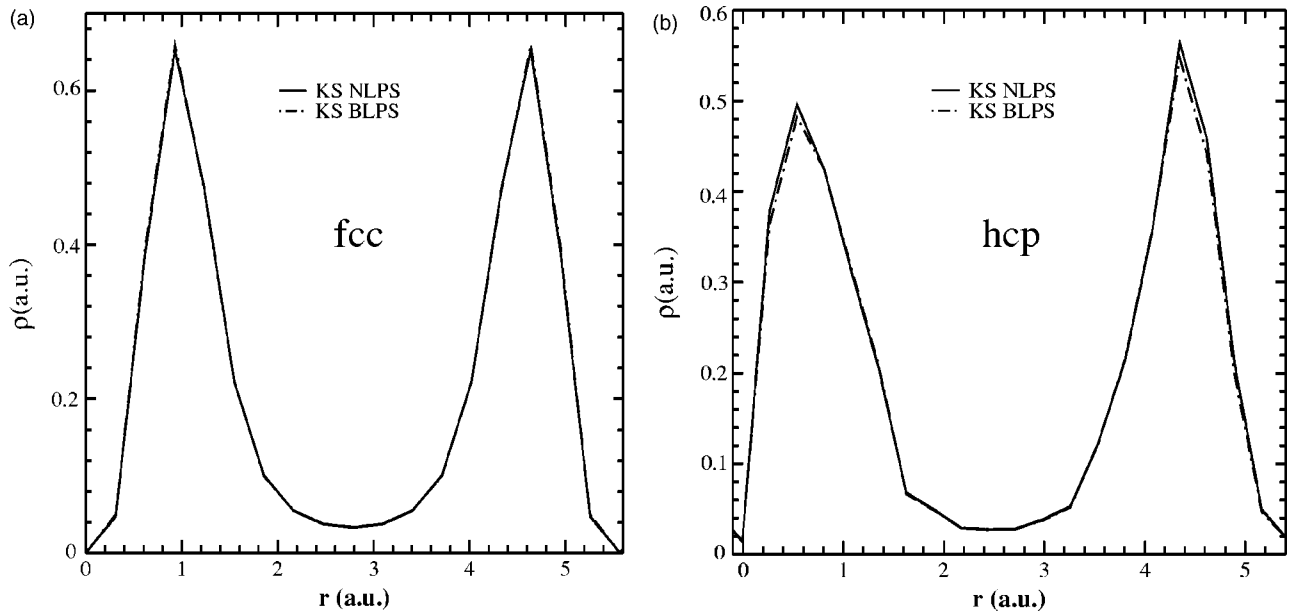

FIG. 5. KS-NLPS (solid) and KS-BLPS (dot-dashed) density slices (a) between the two nearest neighbors of fcc Ag and (b) between the two different atoms in the primitive unit cell for hcp Ag.

BLPS. The EOSs of Ag derived from these BLPSs are of course distinctly different from each other. We can optimize the BLPS by mixing these BLPSs until the final BLPS reproduces the EOS of fcc Ag from the NLPS as closely as possible. Detailed information on the construction of the BLPS for Ag from $v'_{\mathrm{bulk}}(g)$ data is available as a separate Electronic Physics Auxiliary Publication Service (EPAPS) document (see Ref. 43).

Our best BLPS in reciprocal space is plotted in Fig. 4 (Sec. II D). It matches the form factors of fcc and hcp phases very well for $g<4.0$ Å^{-1} and strikes a compromise between the form factors of the two phases for 4.0 Å$^{-1}<g<8.0$ Å^{-1}. The corresponding real space BLPS and ALPS are shown in Fig. 1 (Sec. II A), where we see that they are strongly repulsive within 0.4 a.u., in order to force the $4d$ electrons out of the core region. As r increases, both the ALPS and the BLPS decrease until they hit a minimum of about -12 to -14 hartree at $\sim$0.8 to $\sim$0.85 bohr. The minimum of the BLPS is shallower than that of the ALPS. Beyond 1 bohr, the ALPS closely resembles the d channel of the NLPS; the BLPS increases more slowly as r increases. We call this final, optimized BLPS simply BLPS in the following.

III. TESTING THE BLPS WITHIN KS-DFT

We first test the BLPS derived from the above procedure in KS-DFT calculations, by comparing the resulting densities, EOSs, and static structural properties to those from the NLPS. Due to the strongly repulsive nature of the BLPS for Ag (see Fig. 1), a much higher kinetic-energy cutoff of 2600 eV is used in order to converge the total energy to 5 meV/atom. All other calculational details are the same as in Sec. II B.

Results

The self-consistent density obtained using the ALPS within KS-DFT was of very poor quality. The charge density is too high in the outer core region (about 1 a.u. from the nucleus) with a peak of about 1 a.u. instead of $\sim$0.6 a.u. found with the NLPS (see Fig. 5). This is due to the ALPS being too attractive at $\sim$1 bohr from the nucleus [see Fig. 1(b)]. By design, the BLPS reproduces the density from the NLPS very well. Figure 5 shows that the density of the BLPS is almost indistinguishable from that of the NLPS for both fcc and hcp Ag.

We then used the BLPS to calculate the EOSs of fcc and hcp Ag. Note that we did not use the KS-NLPS EOS data of hcp Ag to refine the BLPS from the atomic form factors [see EPAPS document (Ref. 43)]. Thus the transferability of the BLPS is tested somewhat by assessing the accuracy of the EOS for hcp Ag. The computed BLPS, NLPS, and ALPS EOSs are depicted in Fig. 6. The resulting EOSs from the BLPS for both structures are fairly close to those from the NLPS, although discrepancies still exist for volumes between 16 and 24 Å^3. The fcc BLPS EOS matches the fcc NLPS EOS very well for volumes less than 16 Å^3, while the hcp EOS rises too steeply at small volumes when the BLPS is used. By contrast, use of the ALPS in KS-LDA leads to a completely unphysical EOS, with no minimum in either EOS, and where the total energy monotonically increases with increasing volume. Thus, the BLPS represents a significant improvement over the ALPS.

We then fit the EOS data from the BLPS KS-LDA calculations to Murnaghan's equation of state [Eq. (2)] to obtain the equilibrium volumes V_0, bulk moduli B_0, and equilibrium energies E_{min}, which are given in Table I. The BLPS overestimates V_0 by $\sim$1.4% for the fcc phase and $\sim$4.3% for the hcp phase relative to the NLPS. B_0 is also too large, with errors of $\sim$12% for fcc and $\sim$18% for hcp, respectively. The

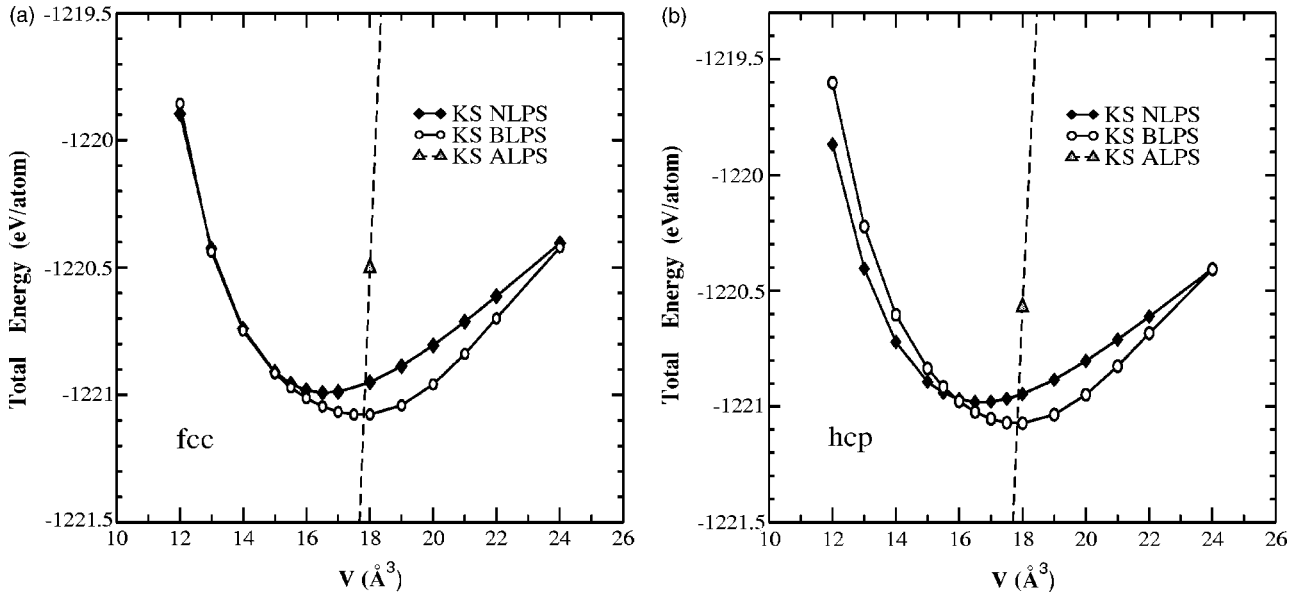

FIG. 6. KS-LDA total energies (eV/atom) vs atomic volume (Å^3) for (a) fcc Ag; (b) hcp Ag. Here we compare NLPS (solid diamonds) to BLPS (open circles) to ALPS (opaque triangles). The NLPS EOS is shifted down by 235.15 eV/atom, while the ALPS EOS is shifted up by 232.733 eV/atom. On this scale, only one data point is present for the ALPS.

fcc phase is still predicted to be the ground state, although the energy difference between fcc and hcp phases is slightly larger than for the NLPS. Unfortunately, the cohesive energy cannot be readily calculated from either the ALPS or the BLPS. We found that using the ALPS or BLPS in atomic KS-DFT calculations led to unphysical results, where the eigenvalue of the 5*s* orbital is much lower (by ~76.6 eV for the ALPS and by ~54.1 eV for the BLPS) than that of the 4*d* orbital. This is certainly an indication of the limited transferability of this type of LPS for Ag. Neither the one derived from the atom, nor the one derived from bulk crystals can describe the $4d^{10}5s^1$ state of the atom properly. Note that the WP approach does not constrain the pseudopotential to reproduce atomic energy eigenvalues as other pseudopotential construction methods do. Thus, there is no reason to expect that the total energy of the atom, nor its orbital energies, will be correctly reproduced. The purpose of the BLPS is to be used in OF-DFT condensed-matter calculations, where atomic energy eigenvalues do not enter.

IV. APPLICATION OF THE BLPS IN OF-DFT

While this BLPS is unsuitable for atomic (and probably molecular) Ag species, our actual goal was to study bulk Ag with OF-DFT. Since we have shown that this BLPS produces a fair description of Ag's bulk properties within KS-DFT, we should see that the majority of the remaining error in OF-DFT will be in the choice of KEDF, which is the only difference between KS-DFT and OF-DFT when the same pseudopotentials are used. We explored the family of KEDFs comprised of the full von Weizsäcker KEDF,[44] T_{vW}, and a partial contribution from the Thomas–Fermi KEDF,[45] T_{TF}. The resulting von Weizsäcker-λ-Thomas–Fermi (vW-λTF) KEDF, $T_{\mathrm{vW}}+\lambda T_{\mathrm{TF}}$, where λ is a constant coefficient, is simply an extension of the von Weizsäcker KEDF.[46] We also used the LR-based[25] Wang–Teter (WT) KEDF.[16] The more accurate LR-based Wang–Govind–Carter (WGC) KEDF was not used due to convergence issues observed for systems involving highly localized electron distributions.[15,23]

A. Calculational details

In our OF-DFT calculations, the Hartree term is computed in reciprocal space, the pseudopotential term is calculated in real space, and the kinetic-energy terms are evaluated in both real and reciprocal space. In particular, the TF term is evaluated in real space, the vW and linear-response terms are evaluated partly in both spaces. The LDA is used for the electron exchange-correlation term, which is already $O(N)$ scaling in real space due to its short-range nature. $O(N\ln N)$ scaling fast Fourier transforms (FFTs)[47] are used to transform, e.g., electron density, back and forth between real and reciprocal space.

In order to compare more directly with the CASTEP KS calculations predictions presented earlier, we define our real-space grid in exactly the same way as CASTEP 4.2 (Ref. 48) for the OF-DFT calculations. In particular, we use a double-fine grid, where the maximum integer multiple of the momentum vector along direction $i(i=x,y,z)$ is calculated as

$$n_i = 3\frac{L_i}{2\pi}\sqrt{E_{\mathrm{cut}}}. \tag{11}$$

Here, L_i is the length (in bohr) of the simulation cell in one direction and E_{cut} is an energy cutoff parameter in rydbergs. Based on Eq. (11), the maximum energy of the plane wave on the reciprocal space grid is nine times E_{cut}. In this work, E_{cut} is set to 88.20 Ry (1200 eV, as in the earlier KS-NLPS calculations). When the pseudopotential energy is calculated, all the points in the Fourier grid are used in order to adequately represent the very repulsive BLPS in the plane wave basis set. Hence, the maximum energy of the plane waves used reaches ~10 000 eV. A second-order damped dynamics method is employed to minimize the total

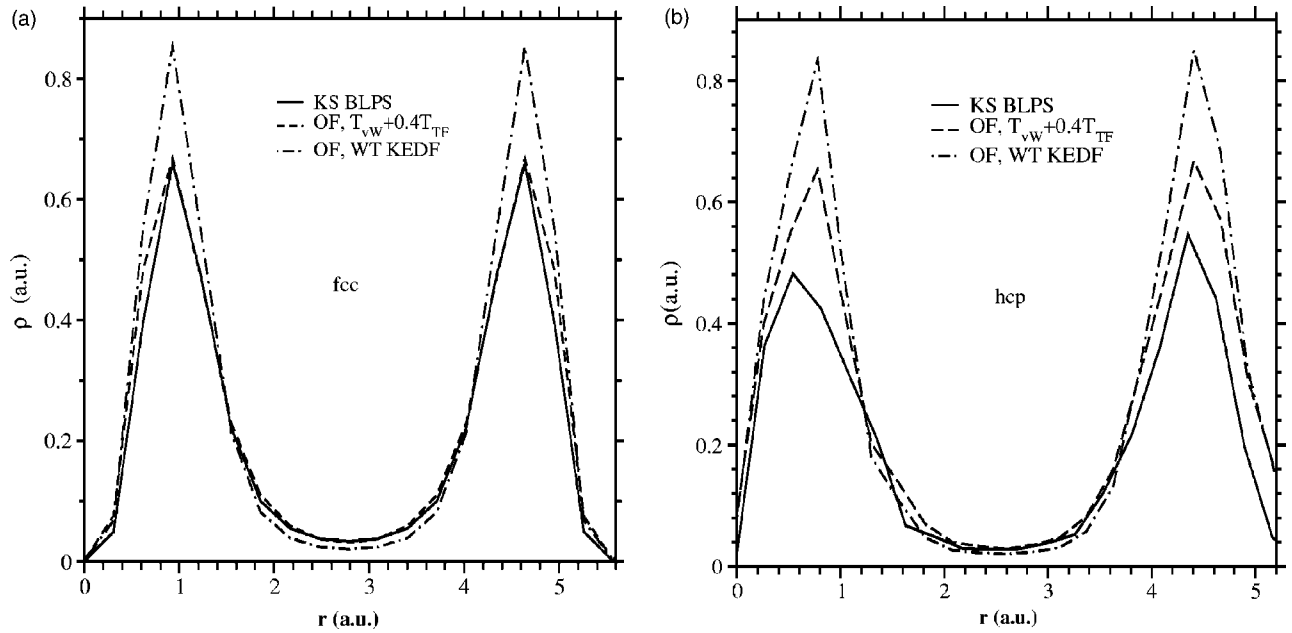

FIG. 7. LDA density slices between (a) nearest neighbors in fcc Ag and (b) the two different atoms in the primitive hcp cell. We compare KS (solid) to OF/$\{T_{vW}+0.4T_{TF}\}$ (dashed) to OF/WT KEDF (dot-dashed).

energy,[14,20] with a convergence criterion of 2.5×10^{-6} eV/atom.

In these OF-DFT calculations, the standard four-atom cubic unit cell is used for fcc Ag. A four-atom orthorhombic cell in ratio $a:b:c=1:\sqrt{3}:1.656$ is used for hcp Ag. The fractional coordinates of the four atoms in this hcp unit cell are (0, 0, 0), $(\frac{1}{2},\frac{1}{2},0)$, $(\frac{1}{2},\frac{1}{6},\frac{1}{2})$, and $(0,\frac{2}{3},\frac{1}{2})$.

B. Results

Figure 7 compares the variational densities from OF-DFT (ρ^{OF}) to those from KS-DFT calculations (ρ^{KS}). By varying λ in the vW-λTF KEDF, we found that λ=0.4 yielded the best densities. Figure 7(a) compares the ρ^{OF} and ρ^{KS} between the nearest neighbors of fcc Ag using the λ=0.4 KEDF and using the WT KEDF. We see that ρ^{OF} derived from the $T_{vW}+0.4T_{TF}$ closely resembles ρ^{KS}, while enforcement of the correct LR behavior does not improve ρ^{OF}. Instead, the quality of ρ^{OF} from the WT KEDF is worse, significantly overestimating the density in the outer core region at ~1 bohr from the nucleus. Figure 7(b) depicts ρ^{OF} and ρ^{KS} between two atoms with fractional coordinates $(\frac{1}{2},\frac{1}{2},0)$ and $(\frac{1}{2},\frac{1}{6},\frac{1}{2})$, which are equivalent to the two different sets of atoms in the primitive hcp cell of Sec. II B. Again, we see that ρ^{OF} from the $T_{vW}+0.4T_{TF}$ is better than that from the WT KEDF, although both exhibit large deviations from ρ^{KS}, indicating that neither KEDF can satisfactorily describe both fcc and hcp Ag.

We also attempted to calculate the EOS of fcc Ag with OF-DFT. Figure 8 displays the OF-DFT predictions using the two KEDFs above, where we see that both KEDFs yield unphysical EOSs. The $T_{vW}+0.4T_{TF}$ total energy monotonically increases with volume, but does not exhibit a minimum. The opposite trend is observed for the WT KEDF EOS, with the total energy unphysically decreasing with increased volume. Again, no minimum in the EOS is observed. This illustrates a complete breakdown of these simple KEDFs when applied to systems containing both localized and delocalized electron densities.

V. CONCLUSIONS

A new local pseudopotential (BLPS) for bulk Ag was constructed with our recently developed method of inverting the KS equations in a bulk crystalline environment. By design, this BLPS produces KS-DFT densities in good agree-

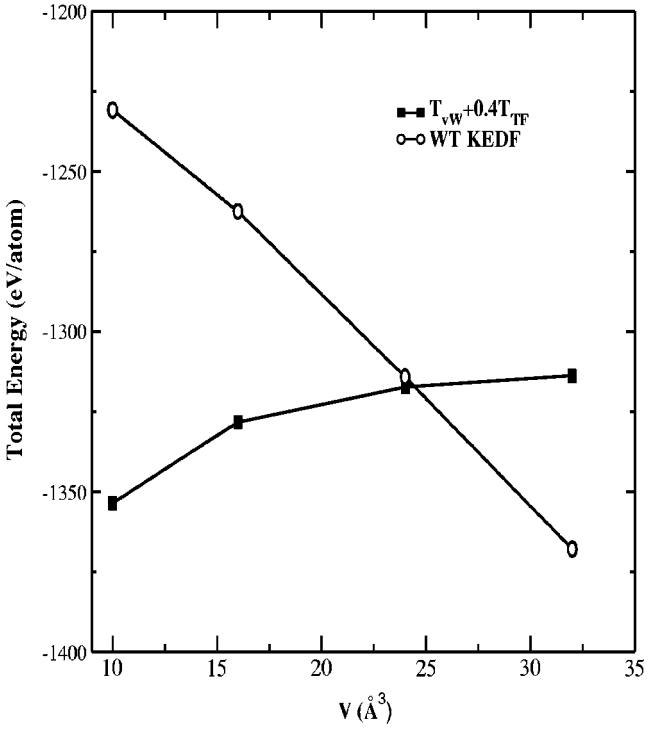

FIG. 8. OF-BLPS total energies vs atomic volume for fcc Ag: $T_{vW}+0.4T_{TF}$ (solid squares) vs WT KEDF (open circles).

ment with those obtained within KS-DFT using a high-quality nonlocal pseudopotential (NLPS). The equilibrium bulk properties yielded by the BLPS are in fair agreement with those obtained using the NLPS. Although we have shown here that it is possible to construct a reasonable local pseudopotential to represent both a *d* and *s* shell of electrons, current KEDFs are not sufficiently robust to predict properties of materials containing simultaneously delocalized (*sp*) and localized (*d*) electron densities. For example, although the combination of this BLPS with the $T_{vW}+0.4T_{TF}$ KEDF within OF-DFT produces an accurate density, the EOS produced has no minimum. Enforcing correct LR behavior of a uniform gas is not helpful, as evidenced by the poor WT KEDF density. This is not surprising, since the highly localized 4*d* electrons are far from small perturbations away from a uniform gas, upon which the LR-based KEDFs are based. Unfortunately, the EOSs obtained in OF-DFT from both KEDFs contain unacceptably large errors. Nevertheless, the respectable behavior exhibited by this BLPS within KS theory paves the way for further improvement of KEDFs to treat transition metals in the future, as the remaining errors in OF-DFT can be ascribed to deficiencies primarily in the KEDF. Use of this BLPS will provide a good test case for future KEDF development.

ACKNOWLEDGMENTS

We thank Professor Yan Alexander Wang (University of British Columbia) for providing the ALPS and Accelrys, Inc. for providing the CASTEP software. Financial support for this project was provided by the DOD-MURI program and the National Science Foundation.

[1]P. Hohenberg and W. Kohn, Phys. Rev. **136**, B864 (1964).
[2]W. Kohn and L. J. Sham, Phys. Rev. **140**, A1133 (1965).
[3]S. Kurth, J. P. Perdew, and P. Blaha, Int. J. Quantum Chem. **75**, 889 (1999).
[4]W. E. Pickett, Comput. Phys. Rep. **9**, 115 (1989).
[5]N. W. Ashcroft and N. D. Mermin, *Solid State Physics* (Saunders, Orlando, 1976).
[6]A. Stathopoulos, S. Öğüt, Y. Saad, J. Chelikowsky, and H. Kim, Comput. Sci. Eng. **2**, 19 (2000).
[7]S. Goedecker, Rev. Mod. Phys. **71**, 1085 (1999).
[8]F. Shimojo, R. K. Kalia, A. Nakano, and P. Vashishta, Comput. Phys. Commun. **140**, 303 (2001).
[9]W. Kohn, Phys. Rev. Lett. **76**, 3168 (1996).
[10]M. Foley, E. Smargiassi, and P. A. Madden, J. Phys.: Condens. Matter **6**, 5231 (1994); M. Foley, Ph. D. thesis, Oxford University, UK (1995); E. Smargiassi and P. A. Madden, Phys. Rev. B **51**, 117 (1995); S. C. Watson, Ph. D. thesis, Oxford University, UK (1996); B. J. Jesson, M. Foley, and P. A. Madden, Phys. Rev. B **55**, 4941 (1997); J. A. Anta, B. J. Jesson, and P. A. Madden, *ibid.* **58**, 6124 (1998); N. Govind, J. Wang, and H. Guo, *ibid.* **50**, 11 175 (1994); N. Govind, J. L. Mozos, and H. Guo, *ibid.* **51**, 7101 (1995); V. Shah, D. Nehete, and D. G. Kanhere, J. Phys.: Condens. Matter **6**, 10 773 (1994); D. Nehete, V. Shah, and D. G. Kanhere, Phys. Rev. B **53**, 2126 (1996); V. Shah and D. G. Kanhere, J. Phys.: Condens. Matter **8**, L253 (1996); V. Shah, D. G. Kanhere, C. Majumder, and D. G. Das, *ibid.* **9**, 2165 (1997); A. Vichare and D. G. Kanhere, *ibid.* **10**, 3309 (1998); P. Blaise, S. A. Blundell, C. Guet, Phys. Rev. B **55**, 15 856 (1997); A. Aguado, J. M. López, J. A. Alonso, and M. J. Stott, J. Chem. Phys. **111**, 6026 (1999); A. Aguado, J. M. López, J. A. Alonso, and M. J. Stott, J. Phys. Chem. **105**, 2386 (2001); S. C. Watson and E. A. Carter, Comput. Phys. Commun. **128**, 67 (2000).
[11]S. C. Watson and P. A. Madden, PhysChemComm **1**, 1 (1998).
[12]M. Fago, R. H. Hayes, E. A. Carter, and M. Ortiz, Phys. Rev. B **70**, 10 0102 (2004).
[13]Y. Tal and R. F. W. Bader, Int. J. Quantum Chem., Symp. **12**, 153 (1978); P. K. Chattaraj and B. M. Deb, J. Sci. Ind. Res. **43**, 238 (1984); E. Chacón, J. E. Alvarellos, and P. Tarazona, Phys. Rev. B **32**, 7868 (1985); P. García-González, J. E. Alvarellos, and E. Chacón, *ibid.* **53**, 9509 (1996); P. García-González, J. E. Alvarellos, and E. Chacón, *ibid.* **57**, 4857 (1998); P. García-González, J. E. Alvarellos, and E. Chacón, Phys. Rev. A **54**, 1897 (1996); P. García-González, J. E. Alvarellos, and E. Chacón, *ibid.* **57**, 4192 (1998).
[14]Y. A. Wang and E. A. Carter, in *Theoretical Methods in Condensed Phase Chemistry* (Kluwer, Dordrecht, 2000), pp. 117–184.
[15]B. Zhou, V. L. Lignères, and E. A. Carter, J. Chem. Phys. **122**, 44103 (2005).
[16]L.-W. Wang and M. P. Teter, Phys. Rev. B **45**, 13 196 (1992).
[17]M. Pearson, E. Smargiassi, and P. A. Madden, J. Phys.: Condens. Matter **5**, 3321 (1993); E. Smargiassi and P. A. Madden, Phys. Rev. B **49**, 5220 (1994); M. Foley and P. A. Madden, Phys. Rev. B **53**, 10 589 (1996).
[18]F. Perrot, J. Phys.: Condens. Matter **6**, 431 (1994).
[19]Y. A. Wang, N. Govind, and E. A. Carter, Phys. Rev. B **58**, 13 465 (1998); **64**, 129901 (E) (2001).
[20]Y. A. Wang, N. Govind, and E. A. Carter, Phys. Rev. B **60**, 16 350 (1999); **64**, 089 903 (E) (2001).
[21]S. Watson, B. J. Jesson, E. A. Carter, and P. A. Madden, Europhys. Lett. **41**, 37 (1998).
[22]J. A. Anta and P. A. Madden, J. Phys.: Condens. Matter **11**, 6099 (1999).
[23]B. Zhou, Y. A. Wang, and E. A. Carter, Phys. Rev. B **69**, 125 109 (2004).
[24]W. C. Topp and J. J. Hopfield, Phys. Rev. B **7**, 1295 (1973); J. A. Appelbaum and D. R. Hamann, *ibid.* **8**, 1777 (1973); M. Schlüter, J. R. Chelikowsky, S. G. Louie, and M. L. Cohen, *ibid.* **12**, 4200 (1975); Th. Starkloff and J. D. Joannopoulos, *ibid.* **16**, 5212 (1977); J. Harris and R. O. Jones, Phys. Rev. Lett. **41**, 191 (1978); J. Ihm and M. L. Cohen, Solid State Commun. **29**, 711 (1979); L. Goodwin, R. J. Needs, and V. Heine, J. Phys.: Condens. Matter **2**, 351 (1990); F. Nogueira, C. Fiolhais, J. He, J. P. Perdew, and A. Rubio, J. Phys.: Condens. Matter **8**, 287 (1996); D. J. González, L. E. González, J. M. López, and M. J. Stott, Phys. Rev. B **65**, 184 201 (2002); B. Wang and M. J. Stott, *ibid.* **68**, 19 5102 (2003).
[25]K. S. Singwi and M. P. Tosi, Solid State Phys. **36**, 177 (1981); J. Hafner, *From Hamiltonians to Phase Diagrams: The Electronic and Statistical-Mechanical Theory of sp-Bonded Metals and Alloys* (Springer-Verlag, Berlin, 1987); D. Pines and P. Nozières, *The Theory of Quantum Liquids* (Addison-Wesley, New York, 1989), Vol. 1; D. G. Pettifor, *Bonding and Structures of Molecules and Solids* (Clarendon, Oxford, 1995).
[26]D. M. Ceperley and B. J. Alder, Phys. Rev. Lett. **45**, 566 (1980).
[27]J. P. Perdew and A. Zunger, Phys. Rev. B **23**, 5048 (1981).
[28]Y. Wang and R. G. Parr, Phys. Rev. A **47**, R1591 (1993).
[29]W. A. Harrison, *Solid State Theory* (Dover, New York, 1980); W. A. Harrison, *Electronic Structure and the Properties of Solids* (Dover, New York, 1989).
[30]N. Troullier and J. L. Martins, Phys. Rev. B **43**, 1993 (1991).
[31]M. Fuchs and M. Scheffler, Comput. Phys. Commun. **119**, 67 (1999).
[32]L. Kleinman and D. M. Bylander, Phys. Rev. Lett. **48**, 1425 (1982).
[33]X. Gonze, R. Stumpf, and M. Scheffler, Phys. Rev. B **44**, 8503 (1991).
[34]Y. A. Wang and E. A. Carter (unpublished).
[35]M. C. Payne, M. P. Teter, D. C. Allan, T. A. Arias, and J. D. Joannopoulos, Rev. Mod. Phys. **64**, 1045 (1992); M. D. Segall, P. J. D. Lindan, M. J. Probert, C. J. Pickard, P. J. Hasnip, S. J. Clark, and M. C. Payne, J. Phys.: Condens. Matter **14**, 2717 (2002); M. D. Segall, C. J. Pickard, R. Shah, and M. C. Payne, Mol. Phys. **89**, 571 (1996).
[36]J. Donohue, *The Structure of the Elements* (Wiley, New York, 1974).
[37]H. J. Monkhorst and J. D. Pack, Phys. Rev. B **13**, 5188 (1976).
[38]F. D. Murnaghan, Proc. Natl. Acad. Sci. U.S.A. **30**, 244 (1944).
[39]N. Takeuchi, C. T. Chan, and K. M. Ho, Phys. Rev. B **40**, 1565 (1989).
[40]D. R. Hamann, M. Schlüter, and C. Chiang, Phys. Rev. Lett. **43**, 1494 (1979); G. B. Bachelet and M. Schlüter, Phys. Rev. B **25**, 2103 (1982); L. Kleinman, *ibid.* **21**, 2630 (1980).
[41]C. Kittel, *Introduction to Solid State Physics* (Wiley, New York, 1996).
[42]*CRC Handbook of Chemistry and Physics*, 82nd ed. edited by David R. Lide, (CRC, Boca Raton, FL, 2001).
[43]See EPAPS Document No. E-JCPSA6-122-308520 for details on the construction of the BLPS for Ag. A direct link to this document may be found in the online article's HTML reference section. The document may also be

reached via the EPAPS homepage (http://www.aip.org/pubservs/epaps.html or from ftp.aip.org in the directory /epaps/. See the EPAPS homepage for more information.
[44]C. F. von Weizsäcker, Z. Phys. **96**, 431 (1935).
[45]L. H. Thomas, Proc. Cambridge Philos. Soc. **23**, 542 (1927); E. Fermi, Rend. Accad. Naz. Lincei **6**, 602 (1927); E. Fermi, Z. Phys. **48**, 73 (1928); P. A. M. Dirac, Proc. Cambridge Philos. Soc. **26**, 376 (1930); N. H. March, Adv. Phys. **6**, 1 (1957).
[46]J. Goodisman, Phys. Rev. A **1**, 1574 (1970); P. K. Acharya, L. J. Bartolotti, S. B. Sears, and R. G. Parr, Proc. Natl. Acad. Sci. U.S.A. **77**, 6978 (1980); J. L. Gázquez, and J. Robles, J. Chem. Phys. **76**, 1467 (1982).
[47]W. H. Press, S. A. Teukolsky, W. T. Vetterling, and B. P. Flannery, *Numerical Recipes in Fortran* (Cambridge University Press, Cambridge, 1992).
[48]P. Lindan, The Guide 2.0 to CASTEP (covering version 4.2), Daresbury Laboratory, Warrington WA4 4AD, UK, 2000.